J|A|C|S
ARTICLES
Published on Web 01/15/2005

Packing and Viscoelasticity of Polyunsaturated ω-3 and ω-6 Lipid Bilayers as Seen by ^{2}H NMR and X-ray Diffraction

Kannan Rajamoorthi,[†,⊥] Horia I. Petrache,[§] Thomas J. McIntosh,[∥] and Michael F. Brown*[,†,‡]

Contribution from the Departments of Chemistry and Physics, University of Arizona, Tucson, Arizona 85721; Laboratory of Physical and Structural Biology, NICHD, National Institutes of Health, Bethesda, Maryland 20892; and Department of Cell Biology, Duke University School of Medicine, Durham, North Carolina 27708

Received June 15, 2004; E-mail: mfbrown@u.arizona.edu

Abstract: Polyunsaturated phospholipids of the ω-3 and ω-6 classes play key roles in cellular functions, yet their mechanisms of biological action are still a matter of debate. Using deuterium (^{2}H) NMR spectroscopy and small-angle X-ray diffraction, we show how membrane properties are modified by docosahexaenoic (DHA; 22:6) and arachidonic (AA; 20:4) acyl chains of the ω-3 and the ω-6 families, respectively. Structural and dynamical differences due to polyunsaturation are evident in both the ordered and disordered phases of mixed-chain (16:0)(22:6)PC and (16:0)(20:4)PC bilayers. Due to the lower chain melting temperature, the ω-6 AA bilayer is more disordered in the fluid (L_α) state than the ω-3 DHA bilayer; it is thinner with a larger area per lipid. The thermal hysteresis observed for the DHA bilayer may represent the influences of angle-iron conformers in the gel state and back-bended, hairpinlike conformers in the fluid state, consistent with molecular dynamics studies. Interpretation of the ^{2}H NMR order profiles of (16:0-d_{31})(22:6)PC and (16:0-d_{31})(20:4)PC together with X-ray electron density profiles reveals an uneven distribution of mass; i.e., the *sn*-1 saturated chain is displaced toward the membrane center, whereas the *sn*-2 polyunsaturated chain is shifted toward the bilayer aqueous interface. Moreover, the ^{2}H NMR relaxation rates are increased by the presence of ω-6 AA chains compared to ω-3 DHA chains. When evaluated at the same amplitude of motion, relaxation parameters give a naturally calibrated scale for comparison of fluid lipid bilayers. Within this framework, polyunsaturated bilayers are relatively soft to bending and area fluctuations on the mesoscale approaching molecular dimensions. Significant differences are evident in the viscoelastic properties of the ω-3 and ω-6 bilayers, a possibly biologically relevant feature that distinguishes between the two phospholipid classes.

Introduction

Phospholipids having polyunsaturated chains of the ω-3 and ω-6 series[1,2] occur in high proportions in cellular membranes including those of retinal rod outer segments[3], cerebral gray matter,[4] mitochondria,[5] and spermatozoa.[6] Depletion of polyunsaturated fatty acids (PUFAs) has long been associated with cardiovascular disease,[7] visual disorders,[8] cancer,[9] aging,[10] and other apparently unrelated physiological and pathological anomalies. There are two possible hypotheses for the biological role of polyunsaturated lipids of the ω-3 and ω-6 series.[11] In a first scenario, they give rise to messenger molecules through the hydrolytic action of phospholipase A_2 together with cyclooxygenase, lipoxygenase, or cytochrome P-450 monooxygenase enzymes. For instance, arachidonic acid (AA), an ω-6 fatty acid, acts as a precursor in the biosynthesis of prostaglandins, thromboxanes, and leukotrienes.[12] These products modulate cellular functions including platelet aggregation, smooth muscle contraction, and neural excitation.[13] Yet, in

[†] Department of Chemistry, University of Arizona.
[‡] Department of Physics, University of Arizona.
[§] National Institutes of Health.
[∥] Duke University School of Medicine.
[⊥] Present address: BASF Agro Research, P.O. Box 400, Princeton, NJ 08543-0400.

(1) Stillwell, W.; Wassall, S. R. *Chem. Phys. Lipids* **2003**, *126*, 1−27.
(2) Eldho, N. V.; Feller, S. E.; Tristram-Nagle, S.; Polozov, I. V.; Gawrisch, K. *J. Am. Chem. Soc.* **2003**, *125*, 6409−6421.
(3) (a) Salem, N., Jr.; Litman, B.; Kim, H.-Y.; Gawrisch, K. *Lipids* **2001**, *36*, 945−959. (b) Jump, D. B. *J. Biol. Chem.* **2002**, *277*, 8755−8758.
(4) (a) O'Brien, J. S.; Sampson, E. L. *J. Lipid Res.* **1965**, *6*, 545−551. (b) Cotman, C.; Blank, M. L.; Moehl, A.; Snyder, F. *Biochemistry* **1969**, *8*, 4606−4612.
(5) Witting, L. A.; Harvey, C. C.; Century, B.; Horwitt, M. K. *J. Lipid Res.* **1961**, *2*, 412−422.
(6) Lenzi, A.; Gandini, L.; Maresca, V.; Rago, R.; Sagrò, P.; Dondero, F.; Picardo, M. *Mol. Hum. Reprod.* **2000**, *6*, 226−231.
(7) (a) Glomset, J. A. *N. Engl. J. Med.* **1985**, *312*, 1253−1254. (b) Sellmayer, A.; Hrboticky, N.; Weber, P. C. *Lipids* **1999**, *34*, S13−S18.
(8) (a) Neuringer, M.; Connor, W. E.; Lin, D. S.; Barstad, L.; Luck, S. *Proc. Natl. Acad. Sci. U.S.A.* **1986**, *83*, 4021−4025. (b) Neuringer, M. *Am. J. Clin. Nutr.* **2000**, *71*, 256S−267S.
(9) (a) Borgeson, C. E.; Pardini, L.; Pardini, R. S.; Reitz, R. C. *Lipids* **1989**, *24*, 290−295. (b) Henderson, C. D.; Black, H. S.; Wolf, Jr., J. E. *Lipids* **1989**, *24*, 502−505.
(10) Harman, D. *Proc. Natl. Acad. Sci. U.S.A.* **1981**, *78*, 7124−7128.
(11) (a) Brown, M. F.; Gibson, N. J. In *Essential Fatty Acids and Eicosanoids*; Sinclair, A., Gibson, R., Eds.; American Oil Chemist's Society Press: Champaign, Illinois, 1992; pp 134−138. (b) Salem, N.; Niebylski, C. D. In *Essential Fatty Acids and Eicosanoids*; Sinclair, A., Gibson, R., Eds.; American Oil Chemist's Society Press: Champaign, Illinois, 1992; pp 84−86.
(12) (a) Lagarde, M.; Gualde, N.; Rigaud, M. *Biochem. J.* **1989**, *257*, 313−320. (b) Stinson, S. C. *Chem. Eng. News* **1989**, *67*, 37−70.

 10.1021/ja046453b CCC: $30.25

contrast to AA, evidence has not been obtained for the presence of significant metabolites of docosahexaenoic acid (DHA), an ω-3 fatty acid.[3,14] Differences in the properties of AA versus DHA lipids are of great biochemical interest.[15] DHA itself is known to be a potent inhibitor of cyclooxygenase and to affect prostaglandin but not leukotriene biosynthesis.[16] DHA (and phytanic acid) functions as a ligand for the retinoid X receptor, a nuclear hormone receptor acting as a ligand-activated transcription factor, which may account for some of its biological effects.[17] Other studies have shown that DHA influences the Cl^- channel implicated in cystic fibrosis[18] as well as neuronal K^+ channels,[19] consistent with a messenger function. Moreover, DHA is specifically released in response to neurotransmitters such as serotonin[20] and brain injury.[21]

A deficiency of DHA has been shown to affect spatial learning and retinal function in rats and humans,[8,22] suggesting an essential role in brain maturation and neural functions. The high enrichment of the mammalian brain with DHA during late gestation and neonatal development results in its massive introduction into membrane phospholipids, where it comprises 30−50% of the total fatty acids.[23] This large-scale incorporation suggests an alternative hypothesis with regard to the mode of action of lipids containing polyunsaturated fatty acids. Namely, the high degree of polyunsaturation in neuronal and retinal membranes may confer distinct lipid bilayer properties which govern the functions of integral membrane proteins, for instance G protein-coupled receptors such as rhodopsin.[24] Compared to less unsaturated lipids, polyunsaturated bilayers have a reduced thickness in the fluid state, corresponding to an increased area per molecule at the aqueous interface, a result of the greater acyl chain disorder.[25] In a series of lipid substitution experiments, consisting of variations of acyl polyunsaturation and headgroups, nonspecific biophysical properties of the membrane bilayer have been shown to influence the conformational energetics of rhodopsin.[24] This work has led to a new biomembrane model,[26] in which the spontaneous curvature of the bilayer lipids depends on acyl chain unsaturation as well as the headgroup type. Matching of the bilayer spontaneous curvature to the boundary curvature imposed by an integral protein leads to an elastic coupling between the protein and the surrounding membrane, thereby explaining the lipid influences on biological function.[26] As a result, DHA chains in combination with zwitterionic (PC, PE) and anionic (PS) phospholipid headgroups may be involved in tuning the bilayer spontaneous curvature under the influence of H_3O^+ ions (pH) near the membrane surface.[27]

However, the different effects of ω-3 and ω-6 polyunsaturated phospholipids may be difficult to explain within such a framework. Measurements of biophysical properties of AA and DHA polyunsaturated fatty acids are thus of considerable interest.[1,2,28] Here we report comparative studies of phosphatidylcholines containing either arachidonic acid (20:4ω-6) or docosahexaenoic acid (22:6ω-3) at position *sn*-2 and a saturated palmitic acid chain (16:0) at position *sn*-1. Comparison with phosphatidylcholines having only saturated or monounsaturated fatty acids provides a reference scale[29] for the observed differences between the ω-3 and the ω-6 lipids. In this work we have used deuterium nuclear magnetic resonance (^{2}H NMR) spectroscopy[25,29−32] and small-angle X-ray diffraction[33] to determine the dynamic structure of these lipid bilayers. For the ^{2}H NMR measurements, the *sn*-1 saturated chain has been ^{2}H labeled to act as a probe for the influences of the polyunsaturated *sn*-2 chain on bilayer properties.[25] We first present the equilibrium acyl chain order parameters and the average bilayer structures obtained from ^{2}H NMR and X-ray diffraction, respectively. In terms of the acyl chain packing, as manifested by the ^{2}H NMR order profiles, the polyunsaturated (16:0-d_{31})-(20:4)PC and (16:0-d_{31})(22:6)PC bilayers are distinct from disaturated and monounsaturated bilayers in that an increase in configurational freedom is evident. This finding is in agreement with the X-ray measurements, which reveal an increased area per molecule at the aqueous interface corresponding to reduced bilayer thickness. A displacement of the mass of the PUFA *sn*-2 chain toward the bilayer surface is evident relative to the saturated *sn*-1 chain, which extends further into the bilayer center. We then describe ^{2}H NMR relaxation data which report on molecular motions and viscoelastic properties of the lipid bilayers. While the ^{2}H NMR order parameters of DHA- and AA-containing bilayers are similar, significant differences in the spin−lattice relaxation rates (R_{1Z}) are evident in the chain-melted (fluid) state. Compared to less unsaturated bilayers, the PUFA-containing bilayers are softer to curvature and area deformation on the mesoscopic length scale. Moreover, the AA-containing bilayers appear softer and more deformable than those containing DHA chains, indicating a rather unexpected, perhaps biologically relevant property that differentiates the two fatty acid types. Finally, we discuss the experimentally derived relationship between order and relaxation parameters that highlights the subtle yet well-defined distinction between the physical properties of the ω-3 and ω-6 bilayers.

(13) Needleman, P.; Turk, J.; Jakschik, B. A.; Morrison, A. R.; Lefkowith, J. B. *Annu. Rev. Biochem.* **1986**, *55*, 69−102.
(14) Rapoport, S. I. *J. Pediatr.* **2003**, *143*, S26−S34.
(15) Shikano, M.; Masuzawa, Y.; Yazawa, K.; Takayama, K.; Kudo, I.; Inoue, K. *Biochim. Biophys. Acta* **1994**, *1212*, 211−216.
(16) Corey, E. J.; Shih, C.; Cashman, J. R. *Proc. Natl. Acad. Sci. U.S.A.* **1983**, *80*, 3581−3584.
(17) de Urquiza, A. M.; Liu, S.; Sjöberg, M.; Zetterström, R. H.; Griffiths, W.; Sjövall, J.; Perlmann, T. *Science* **2000**, *290*, 2140−2144.
(18) Freedman, S. D.; Katz, M. H.; Parker, E. M.; Laposata, M.; Urman, M. Y.; Alvarez, J. G. *Proc. Natl. Acad. Sci. U.S.A.* **1999**, *96*, 13995−14000.
(19) Poling, J. S.; Vicini, S.; Rogawski, M. A.; Salem, N. *Neuropharmacology* **1996**, *35*, 969−982.
(20) Garcia, M. C.; Kim, H. Y. *Brain Res.* **1997**, *768*, 43−48.
(21) Homayoun, P.; Parkins, N. E.; Soblosky, J.; Carey, M. E.; de Turco, E. B. R.; Bazan, N. G. *Neurochem. Res.* **2000**, *25*, 269−276.
(22) (a) Uauy, R.; Peirano, P.; Hoffman, D.; Mena, P.; Birch, D.; Birch, E. *Lipids* **1996**, *31*, S167−S176. (b) Greiner, R. S.; Moriguchi, T.; Hutton, A.; Slotnick, B. M.; Salem, N. *Lipids* **1999**, *34*, S239−S243.
(23) Neuringer, M.; Anderson, G.; Connor, W. E. *Annu. Rev. Nutr.* **1988**, *8*, 517−541.
(24) (a) Wiedmann, T. S.; Pates, R. D.; Beach, J. M.; Salmon, A.; Brown, M. F. *Biochemistry* **1988**, *29*, 6469−6474. (b) Gibson, N. J.; Brown, M. F. *Biochemistry* **1993**, *32*, 2438−2454.
(25) Salmon, A.; Dodd, S. W.; Williams, G. D.; Beach, J. M.; Brown, M. F. *J. Am. Chem. Soc.* **1987**, *109*, 2600−2609.
(26) Botelho, A. V.; Gibson, N. J.; Thurmond, R. L.; Wang, Y.; Brown, M. F. *Biochemistry* **2002**, *41*, 6354−6368.
(27) Wang, Y.; Botelho, A. V.; Martinez, G. V.; Brown, M. F. *J. Am. Chem. Soc.* **2002**, *124*, 7690−7701.
(28) (a) Everts, S.; Davis, J. H. *Biophys. J.* **2000**, *79*, 885−897. (b) Brzustowicz, M. R.; Cherezov, V.; Zerouga, M.; Caffrey, M.; Stillwell, W.; Wassall, S. R. *Biochemistry* **2002**, *41*, 12509−12519.
(29) Petrache, H. I.; Salmon, A.; Brown, M. F. *J. Am. Chem. Soc.* **2001**, *123*, 12611−12622.
(30) Rajamoorthi, K.; Brown, M. F. *Biochemistry* **1991**, *30*, 4204−4212.
(31) Barry, J. A.; Trouard, T. P.; Salmon, A.; Brown, M. F. *Biochemistry* **1991**, *30*, 8386−8394.
(32) (a) Holte, L. L.; Peter, S. A.; Sinnwell, T. M.; Gawrisch, K. *Biophys. J.* **1995**, *68*, 2396−2403. (b) Shaikh, S. R.; Cherezov, V.; Caffrey, M.; Stillwell, W.; Wassall, S. R. *Biochemistry* **2003**, *42*, 12028−12037.
(33) (a) McIntosh, T. J.; Magid, A. D.; Simon, S. A. *Biochemistry* **1987**, *26*, 7325−7332. (b) Petrache, H. I.; Tristram-Nagle, S.; Nagle, J. F. *Chem. Phys. Lipids* **1998**, *95*, 83−94.

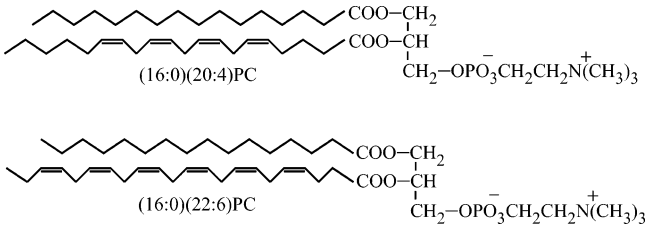

Figure 1. Structures of mixed-chain saturated−polyunsaturated phosphatidylcholines from the ω-6 series (16:0)(20:4)PC and the ω-3 series (16:0)-(22:6)PC. The ^{2}H-labeled saturated chain at the glycerol *sn*-1 position is used to monitor bilayer properties.

Materials and Methods

Synthesis and Preparation of Phospholipids. Egg yolk phosphatidylcholine (egg PC) was procured from Avanti Polar Lipids (Alabaster, SC) and was used without further purification. Polyunsaturated and unsaturated phospholipids were synthesized and characterized as described previously.[30] Briefly, the perdeuterated palmitic acid was prepared by catalytic exchange of deuterium for hydrogen over a 10% Pd-charcoal catalyst (Aldrich, Milwaukee, WI) at 195 °C using ^{2}H gas generated electrolytically from ^2H_2O (99.8%; Aldrich, Milwaukee, WI). The percent incorporation of ^{2}H (95−98%) and the purity (>99%) of the perdeuterated palmitic acid were determined by gas chromatography−mass spectrometry of its methyl ester. The symmetric disaturated phospholipid, 1,2-diperdeuteriopalmitoyl-*sn*-glycero-3-phosphocholine, was synthesized from the anhydride of the perdeuterated palmitic acid and the cadmium adduct of *sn*-glycero-3-phosphocholine.[34] It was then treated with snake venom phospholipase A_2 from *Crotalus adamanteus* (Sigma, St. Louis, MO) to hydrolyze the *sn*-2 perdeuterated palmitoyl chain yielding the lysophospholipid 1-perdeuteriopalmitoyl-*sn*-glycero-3-phosphocholine. The lysophospholipid was reacylated[35] with arachidonic, erucic, or docosahexaenoic acids (Nu Check Prep, Inc., Elysian, MN) in dimethylformamide in the presence of 1,3-dicyclohexylcarbodiimide, 4-hydroxybenzotriazole, and 4-pyrrolidinopyridine to give the mixed-chain phosphatidylcholines (16:0-d_{31})(20:4)PC, (16:0-d_{31})-(22:1)PC, or (16:0-d_{31})(22:6)PC. Phospholipids were then purified by column chromatography on silicic acid (Bio-Sil A, 100−200 mesh; Bio-Rad, Hercules, CA) with a $CHCl_3$/MeOH solvent gradient. They gave single spots upon thin-layer chromatography using $CHCl_3$/MeOH/H_2O (65/35/5) as the mobile phase, followed by charring with 40% H_2SO_4 in EtOH. The isomeric purity of the (16:0-d_{31})(20:4)PC and (16:0-d_{31})(22:6)PC was determined by treatment with phospholipase A_2 from *Crotalus adamanteus* (Sigma, St. Louis, MO). Transesterification of the *sn*-2 hydrolyzed fatty acids with BCl_3/MeOH (Supelco, PA) followed by their identification by gas−liquid chromatography showed negligible acyl migration (<3%). The polyunsaturated lipid chemical structures are indicated in Figure 1.

^{2}H NMR Spectroscopy. Approximately 200 mg of lipids were lyophilized from cyclohexane/$CHCl_3$ (20/1, v/v) in an 8 mm culture tube, followed by addition of an equal weight of 0.067 M sodium phosphate buffer prepared from ^{2}H-depleted ^1H_2O (Aldrich, WI), containing 10^{-4} M EDTA and 0.01 wt % NaN_3, at pH 7.1. The 50% phospholipid dispersions were briefly vortexed (<1 min) and centrifuged. Sample tubes were closed with Teflon plugs and then cut off and sealed with high-melting (90 °C) wax (Petrolite, Tulsa, OK). The samples were stored under argon at −80 °C. Immediately prior to the ^{2}H NMR measurements the samples were heated to above the main phase transition temperature and allowed to stand for approximately 1 h.

Solid-state ^{2}H NMR spectra were recorded on an NMR spectrometer operating at 46.13 MHz for deuterium. The spectrometer was equipped with a home-built high-power probe with a horizontal solenoid coil, an external fast digitizer for quadrature phase detection, and a high-power (kW) radio frequency amplifier (Henry Radio Tempo 2006). The 90 ° pulse length for the spectrometer setup was typically 6 μs. A phase-cycled, quadrupolar echo pulse sequence, $(\pi/2)_x$-τ_1-$(\pi/2)_y$-τ_2-echo was used,[36] with a pulse spacing of 40 μs and a 30 μs delay before data aquisition following the second pulse. The pulse sequence was repeated every 500 ms, and the spectra were acquired using a spectral width (digitization rate) of 500 kHz (dwell time 2 μs). The temperature was monitored using a thermistor placed immediately above the sample coil. The sample was equilibrated at each temperature for at least 30 min before the spectrum was taken. Free induction decays were Fourier transformed at the maximum of the quadrupolar echo, and the ^{2}H NMR spectra were typically not symmetrized, i.e., we did not normally set the imaginary quadrature channel to zero to increase the signal/noise ratio. Any asymmetry of the ^{2}H NMR spectra is due to inhomogeneity of the oscillatory B_1 field strength across the sample placed within the radio frequency coil.

^{2}H NMR Data Analysis and Reduction. Half-moments (M_k) of the powder-type spectra of randomly oriented bilayers were calculated using the equation

$$M_k = \frac{\int_0^\infty \omega^k f(\omega)\, \mathrm{d}\omega}{\int_0^\infty f(\omega)\, \mathrm{d}\omega} \tag{1}$$

where $f(\omega)$ is the spectral intensity at frequency ω. The kth moment is related to the segmental order parameters by

$$M_k = A_k\left(\frac{3\pi}{2}\right)\chi_Q \frac{1}{n_C}\sum_{i=2}^{n_C} |S_{CD}^{(i)}|^k \tag{2}$$

where A_k is a constant proportional to k,[36,37] $\chi_Q = e^2qQ/h$ is the static quadrupolar coupling constant, and $S_{CD}^{(i)}$ is the C−^{2}H bond order parameter of carbon segment i. The moments are useful for a quantitative characterization of the bilayer order, particularly in the gel state where the quadrupolar splittings due to individual carbon segments are not resolved. The first moment (M_1) is proportional to the mean value of S_{CD} over all acyl chain segments[36,37]

$$M_1 = \frac{\pi}{\sqrt{3}}\chi_Q \frac{1}{n_C}\sum_{i=2}^{n_C} |S_{CD}^{(i)}| = \frac{\pi}{\sqrt{3}}\chi_Q \langle |S_{CD}| \rangle \tag{3}$$

and the second moment (M_2) is proportional to the average value of the order parameter squared

$$M_2 = \frac{9\pi^2}{20}\chi_Q^2 \frac{1}{n_C}\sum_{i=2}^{n_C} |S_{CD}^{(i)}|^2 = \frac{9\pi^2}{20}\chi_Q^2 \langle |S_{CD}|^2 \rangle \tag{4}$$

The values of M_1 and M_2 were used to calculate the distribution width[36,37]

$$\Delta_2 = \frac{\langle |S_{CD}|^2 \rangle - \langle |S_{CD}| \rangle^2}{\langle |S_{CD}| \rangle^2} = \frac{20M_2}{27M_1^2} - 1 \tag{5}$$

The ^{2}H NMR spectra in the L_α phase were numerically deconvoluted with the de-Pakeing algorithm[36,38] to obtain subspectra corresponding to the $\theta = 0°$ orientation of the bilayer normal relative to the main magnetic field. The C−^{2}H bond segmental order parameters, $S_{CD}^{(i)}$,

(34) Mason, J. T.; Broccoli, A. V.; Huang, C.-h. *Anal. Biochem.* **1981**, *113*, 96−101.
(35) Liman, U.; O'Brien, D. F. *Biophys. J.* **1988**, *53*, 497a.
(36) Davis, J. H. *Biophys. Biochim. Acta* **1983**, *737*, 117−171.
(37) Brown, M. F. In *Biological Membranes*; Merz, K. M., Roux, B., Eds.; Birkhäuser: Boston, 1996; pp 175−252.
(38) Sternin, E.; Bloom, M.; MacKay, A. L. *J. Magn. Reson.* **1983**, *55*, 274−282.

were evaluated from the residual quadrupolar splittings ($\Delta\nu_Q$) using the relation

$$|\Delta\nu_Q^{(i)}| = \frac{3}{2}\chi_Q |S_{CD}^{(i)}||\, P_2(\cos\theta)| \quad (6)$$

Here $\chi_Q = e^2qQ/h = 167$ kHz,[36] P_2 is the second Legendre polynomial, and θ is the angle between the bilayer normal and the static magnetic field.

Spin−lattice relaxation experiments were carried out using a phase-cycled, composite pulse quadrupolar echo sequence.[39] Thirteen or more different values of the delay time ($\tau = 3$ ms to 1 s) were employed in each case. Recycle times were at least 4 times greater than the longest spin−lattice relaxation time (T_{1Z}) value, and typically 4000 echoes were collected, Fourier transformed, and de-Paked. Spin−lattice (Zeeman) relaxation rates (R_{1Z}) corresponding to each of the resolved splittings were obtained using a three parameter decaying exponential function

$$S(\tau) = S(\infty) - [S(\infty) - S(0)]\exp(-R_{1Z}\tau) \quad (7)$$

to compute the relaxation curve, where $R_{1Z} \equiv 1/T_{1Z}$ and T_{1Z} is the spin−lattice relaxation time.

Mean-Torque Model of Segmental Conformations. The order parameter $S_{CD}^{(i)}$ of carbon segment (i) is the average $\langle 3\cos^2\beta_{PN}^{(i)} - 1\rangle/2$, where $\beta_{PN}^{(i)}$ denotes the angle between the C−^{2}H bond direction (principal axis frame) and the bilayer normal (director axis), and the brackets indicate a time or ensemble average. In what follows, we are interested in the angle $\beta^{(i)}$ between the z-axis of the internal frame perpendicular to the ^{2}H−C−^{2}H plane and the bilayer normal. By considering the distribution function $f(\cos\beta^{(i)})$ that gives the populations of tilt angles $\beta^{(i)}$,[40−42] we can calculate the structurally relevant average $\langle\cos\beta^{(i)}\rangle$ from the measured $\langle\cos^2\beta^{(i)}\rangle$. A conventional diamond-lattice representation of chain conformations gives the segmental projection along the bilayer normal as[40,43]

$$\langle\cos\beta^{(i)}\rangle = {}^1/_2 - S_{CD}^{(i)} \quad (8)$$

Note that, in the limit of an all-trans axially rotating chain, $S_{CD}^{(i)} = -{}^1/_2$ leading to $\langle\cos\beta^{(i)}\rangle = 1$.

In addition a more recent, continuum representation based on a first-order mean-torque model[41,42] gives the analytical result

$$\langle\cos\beta^{(i)}\rangle = \frac{1}{2}\left(1 + \sqrt{\frac{-8S_{CD}^{(i)} - 1}{3}}\right) \quad (9)$$

for $|S_{CD}^{(i)}| > {}^1/_8$. For $|S_{CD}^{(i)}| < {}^1/_8$, numerical results are obtained.[41,42] The correct limiting result for an all-trans rotating chain ($\langle\cos\beta^{(i)}\rangle = 1$) is reproduced as in the above diamond-lattice model. The advantage of the first-order mean-torque model[42] is that it allows conversion of the order parameter profiles $S_{CD}^{(i)}$ into an equivalent mean-torque strength profile as a function of acyl chain segment index i.

Calculation of Structural Parameters. For planar bilayers, the main structural quantities of interest are the average cross-sectional area of the acyl chain $\langle A_C\rangle$ and the average acyl chain length L_C, which are defined and calculated as explained.[29,42] In the present case we are interested in comparing the properties of the mixed-chain, saturated-polyunsaturated PC series to those of the corresponding disaturated series, based on measurements on the saturated *sn*-1 chain (*n*:0). For the plateau region, assuming the segmental cross-sectional area of the saturated acyl chain and the projected length are inversely correlated,[37,40,41] we have

$$\langle A_C^{(n:0)}\rangle = \frac{2V_{CH_2}}{D_M}\left\langle\frac{1}{\cos\beta}\right\rangle \quad (10)$$

where the segment index i is now suppressed. Here V_{CH_2} represents the volume of a methylene group, and $D_M = 2.54$ Å is the length of a virtual bond between carbons $i-1$ and $i+1$. As derived previously,[42] the area factor $q = \langle 1/\cos\beta\rangle$ can be approximated by

$$q \approx 3 - 3\langle\cos\beta\rangle + \langle\cos^2\beta\rangle \quad (11)$$

which involves the first two moments of the orientational distribution function $f(\cos\beta)$. The first moment $\langle\cos\beta\rangle$ is given by eq 9 above, while the second moment is given by[42]

$$\langle\cos^2\beta\rangle = \frac{1 - 4S_{CD}}{3} \quad (12)$$

With the area factor q obtained from eq 11, we then calculate the average cross-sectional area per saturated acyl chain as[29,42]

$$\langle A_C^{(n:0)}\rangle = q\,\frac{2V_{CH_2}}{D_M} \quad (13)$$

For comparison with the disaturated lipids, we also calculate the associated volumetric thickness, defined in relation with the saturated chain volume $V_C^{(n:0)}$ as

$$D_C^{(n:0)} \equiv \frac{V_C^{(n:0)}}{\langle A_C^{(n:0)}\rangle} \quad (14)$$

Note that the partial area $\langle A_C^{(n:0)}\rangle$ and the volumetric thickness $D_C^{(n:0)}$ pertain to the saturated (*n*:0) chain only, and account only for its contribution to the hydrocarbon region. In addition, $D_C^{(n:0)}$ is not necessarily equal to the average chain projection onto the bilayer normal, denoted by $L_C^{(n:0)}$, as discussed in refs 41,42, and 44. The exact relationship between $D_C^{(n:0)}$ and $L_C^{(n:0)}$ depends on the inter-monolayer packing at the bilayer center and, in the case of mixed-chain polyunsaturated lipids, on possible length mismatch between the saturated *sn*-1 chain and the polyunsaturated *sn*-2 chain. For this reason, we report results for both $D_C^{(n:0)}$ and $L_C^{(n:0)}$, together with an additional length, $L_C^{*(n:0)}$.[41,42] The latter gives the chain extent between the second carbon ($i = 2$) and the ω-carbon ($i = n_C$), calculated as a sum of segmental projections $\langle D_i\rangle$ along the bilayer normal,

$$L_C^{*(n:0)} \equiv \langle z^{(2)}\rangle - \langle z^{(n_C)}\rangle = \sum_{i=3,\,5,\ldots}^{n_C-1}\langle D_i\rangle \quad (15)$$

where $\langle z^{(i)}\rangle$ represents the average coordinate of carbon i. The summation in eq 15 is performed over odd values of i only, from $i = 3$ to $n_C - 1$. The chain extent $L_C^{*(n:0)}$ is a well-defined structural parameter but does not account for chain contributions beyond the end carbons C_2 and C_{n_C}. To include these contributions, the conventional approach[25,41,42] defines the chain length (projection) $L_C^{(n:0)}$ as

$$L_C^{(n:0)} = \frac{1}{2}\sum_{i=2,3,\ldots}^{n_C-1}\langle D_i\rangle + \langle D_{n_C-1}\rangle \quad (16)$$

where the sum is now over all carbons from $i = 2$ to $i = n_C - 1$. The

(39) Williams, G. D.; Beach, J. M.; Dodd, S. W.; Brown, M. F. *J. Am. Chem. Soc.* **1985**, *107*, 6868−6873.
(40) Jansson, M.; Thurmond, R. L.; Barry, J. A.; Brown, M. F. *J. Phys. Chem.* **1992**, *96*, 9532−9544.
(41) Petrache, H. I.; Tu, K.; Nagle, J. F. *Biophys. J.* **1999**, *76*, 2479−2487.
(42) Petrache, H. I.; Dodd, S. W.; Brown, M. F. *Biophys. J.* **2000**, *79*, 3172−3192.
(43) (a) Thurmond, R. L.; Dodd, S. W.; Brown, M. F. *Biophys. J.* **1991**, *59*, 108−113. (b) Douliez, J.-P.; Léonard, A.; Dufourc, E. J. *Biophys. J.* **1995**, *68*, 1727−1739.
(44) Nagle, J. F. *Biophys. J.* **1993**, *64*, 1476−1481.

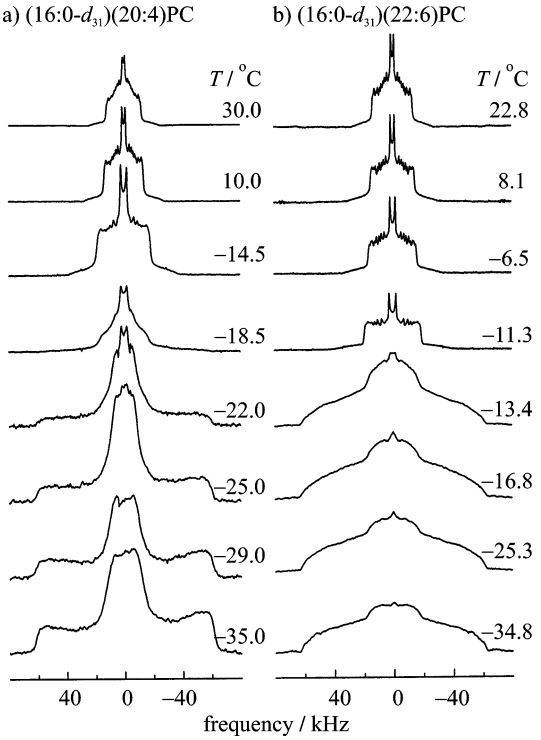

Figure 2. Representative ^{2}H NMR spectra of randomly oriented multilamellar dispersions of (a) (16:0-d_{31})(20:4)PC and (b) (16:0-d_{31})(22:6)PC as a function of decreasing temperature. The samples contained 50 wt % 0.067 M sodium phosphate buffer prepared from ^1H_2O at pH 7. At low temperatures (gel phase), the intensity near ±63 kHz is more pronounced in (16:0-d_{31})(20:4)PC compared to (16:0-d_{31})(22:6)PC. This intensity is due to either the $\theta = 0°$ orientation of all-trans and axially rotating lipids or the $\theta = 90°$ orientation of rigid and nonrotating lipids.

length $L_C^{(n:0)}$ is typically larger than $L_C^{*(n:0)}$ by 1−2 Å but still less than the volumetric thickness $D_C^{(n:0)}$.[42]

X-ray Diffraction. All measurements were carried out essentially as described.[33] In brief, oriented lipid multilayers were prepared by placing a small drop of lipid/chloroform solution on a flat piece of aluminum foil and evaporating the chloroform under a stream of nitrogen. The aluminum foil substrate was given a convex curvature, and the specimen was then mounted in a controlled humidity chamber on a single-mirror (line-focus) X-ray camera. Humidity in the chamber was maintained at 93% with a beaker of saturated Na_2SO_4 solution. The X-ray beam was oriented at a grazing angle to the multilayers on the convex surface of the aluminum foil. X-ray diffraction patterns were recorded on a stack of five sheets of Kodak DEF X-ray film in a flat-plate film cassette. Densitometer traces through the center of each reflection were obtained with a Joyce-Loebl model IIIC microdensitometer. After background subtraction, the integrated intensity, $I(h)$ was multiplied by h (the Lorentz correction factor) due to sample geometry. Phase angles for each reflection were chosen which were consistent with those obtained for other liquid-crystalline phosphatidylcholine bilayers under the same experimental conditions.[33] One-dimensional electron density profiles were then calculated by standard procedures (cf. ref 33).

Results

Deuterium NMR Spectroscopy of ω-3 and ω-6 Polyunsaturated Bilayers. Figure 2 shows ^{2}H NMR powder-pattern spectra of randomly oriented multilamellar dispersions of (16:0-d_{31})(20:4)PC and (16:0-d_{31})(22:6)PC in parts a and b, respectively, each containing 50 wt % H_2O. The spectra consist of a number of overlapping powder patterns arising from the various deuterated acyl chain segments. Measurements are shown both above and below the gel to liquid-crystalline phase transition, reflected by the abrupt changes in the spectra with temperature. Individual chain segments are not clearly distinguished at low temperatures, but these become better resolved as temperature increases.

In the low-temperature gel phase, the ^{2}H NMR spectra present well-defined edges that are more pronounced for AA- than for DHA-containing lipids (Figure 2). Interestingly, the low-temperature ^{2}H NMR spectra of the ω-6 AA bilayer resemble those of the ω-6 (16:0-d_{31})(γ18:3)PC, whereas those of the ω-3 DHA bilayer are more similar to the ω-3 phospholipid (16:0-d_{31})(α18:3)PC, reported in ref 45. The prominent intensity around ±63 kHz is ascribable to the $\theta = 90°$ orientation of rigid, nonrotating acyl chains and/or the $\theta = 0°$ orientation of all-trans, axially rotating lipids. The central component, originating from the reorienting methyl and methylene groups, is larger for the ω-6 AA bilayer than for the ω-3 DHA bilayer, indicating that it may be due to a mismatch of the saturated and PUFA chains at the glycerol *sn*-1 and *sn*-2 positions, respectively. Assuming the mismatch is more pronounced in the gel state for the ω-6 bilayer, the central component is primarily associated with the ends of the saturated *sn*-1 acyl chains near the bilayer center. At higher temperatures, in the L_α state (Figure 2), axially symmetric rotation of the lipids about the bilayer normal (director) occurs. In this case, the sharp spectral features (peaks) correspond to the $\theta = 90°$ orientation of the bilayer normal relative to the main magnetic field direction, and the well-defined shoulders with less intensity arise from the $\theta = 0°$ orientation. The powder-type spectra indicate more gauche conformers of the C^2H_2 segments at higher temperatures (fluid phase) and more trans conformers at lower temperatures (gel phase).

In Figure 3, we plot the first and second moments (M_1 and M_2) as well as the width Δ_2 of the quadrupolar distributions versus temperature, evaluated using eqs 1 and 5. For all-trans, axially rotating lipids, the first moment of the quadrupolar distribution is predicted from eq 3 to be about 1.5×10^5 s^{-1}, close to the actual values. However, it is likely that additional modes of disorder exist in the gel state (vide supra). Evidently, the moments M_1 and M_2 are lower in the gel state for the AA bilayer compared to the DHA bilayer. The phase transition (T_m) between the gel and liquid-crystalline states can be located using any of the M_1, M_2, or Δ_2 parameters, each rendering a particular description of how the transition occurs. In particular, the width Δ_2 emphasizes the sharpness of the order−disorder phase transition for the ω-3 DHA bilayers compared to the ω-6 AA bilayers. Melting of DHA bilayers ($T_m = -12.7$ °C upon cooling and −3 °C upon heating) occurs 10 °C higher than for AA ($T_m = -23$ °C), with a large hysteresis of about 10 °C,[31] while AA bilayers show little or no detectable hysteresis. A similar hysteresis is evident[45] for ω-3 (16:0)(α18:3)PC bilayers in comparison to ω-6 (16:0)(γ18:3)PC. One can conclude that it may be a property of acyl chain mismatch due to ω-3 PUFA chains[31] or more generally due to mismatch of polyethylene and polyallylic groups in bilayers.

For the melted-chain fluid phase, further data reduction is provided by the de-Paking procedure[38] which extracts the signal corresponding to the $\theta = 0°$ orientation from the powder-type

(45) McCabe, M. A.; Griffith, G. L.; Ehringer, W. D.; Stillwell, W.; Wassall, S. R. *Biochemistry* **1994**, *33*, 7203−7210.

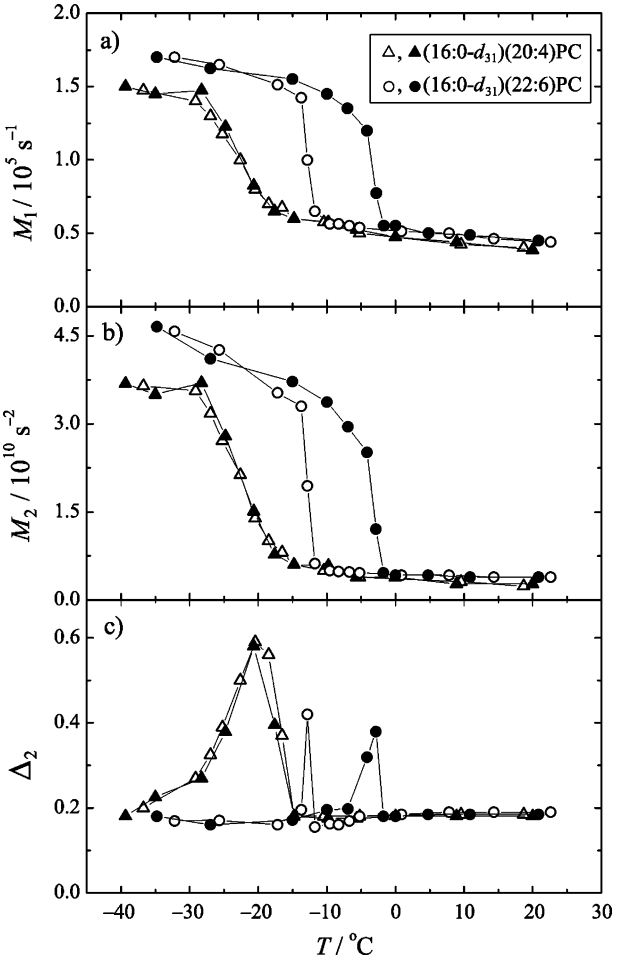

Figure 3. Plots of (a) the first moment (M_1), (b) the second moment (M_2), and (c) the parameter Δ_2 of the ^{2}H NMR spectra as a function of temperature. The symbols correspond to spectra acquired with decreasing temperature (open) and with increasing temperature (filled). All three parameters show a large change in the phase transition region. A sharp phase transition with a large hysteresis is observed for the (16:0-d_{31})-(22:6)PC bilayer, as opposed to a broader transition with little detectable hysteresis for (16:0-d_{31})(20:4)PC.

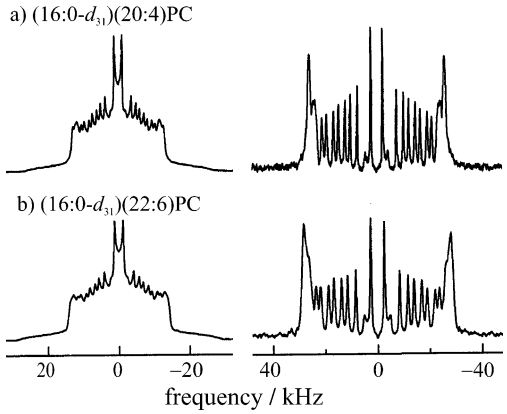

Figure 4. Comparison of representative ^{2}H NMR spectra of aqueous (50 wt % H_2O) multilamellar dispersions of (a) (16:0-d_{31})(20:4)PC and (b) (16:0-d_{31})(22:6)PC in the L_α phase at 15 °C. The powder-type ^{2}H NMR spectra of the random multilamellar dispersions are given at left, and the corresponding de-Paked spectra, at right. At the same absolute temperature, the quadrupolar splittings are larger for the (16:0-d_{31})(22:6)PC bilayer compared to the (16:0-d_{31})(20:4)PC bilayer.

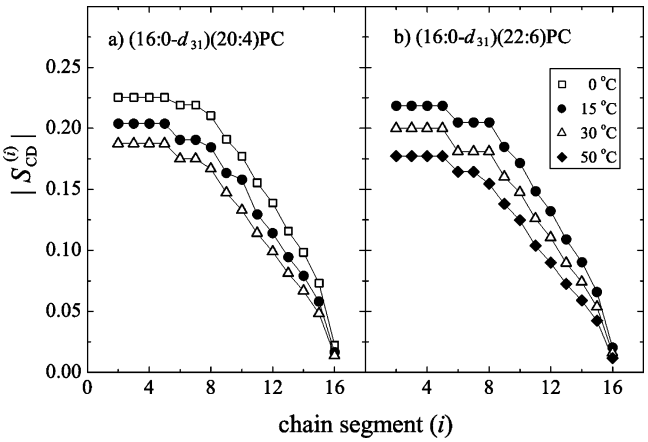

Figure 5. Order parameter profiles of (a) (16:0-d_{31})(20:4)PC and (b) (16:0-d_{31})(22:6)PC at various temperatures in the L_α phase. The $S_{CD}^{(i)}$ values are plotted as a function of chain position i. For both lipids, the *sn*-1 acyl chain order decreases with increasing temperature. At the same absolute temperature the *sn*-1 chain order parameters of (16:0-d_{31})(20:4)PC are *smaller* than those for the *sn*-1 chain of (16:0-d_{31})(22:6)PC.

spectrum. The advantage is that the increased spectral resolution allows more straightforward peak assignments and evaluation of the residual quadrupolar couplings. Figure 4 shows representative powder-type and de-Paked ^{2}H NMR spectra for both of the polyunsaturated lipid bilayers in the fluid state. These spectra are characteristic of melted saturated acyl chains.[37] For both lipids, parts a and b, the smallest splittings correspond to the methyl ends, which are most disordered. The splittings then increase progressively along the chain, ending in an overlap region corresponding to practically equivalent carbon segments next to the glycerol backbone.

Segmental order parameters $S_{CD}^{(i)}$ extracted from fluid-phase spectra using eq 6 are plotted as a function of the chain segment index i in Figure 5. Peak assignments were based on integrated areas with the assumption that the quadrupolar splittings decrease along the chain.[25] These profiles provide a quantitative measure of the orientational ordering of the acyl chains of phospholipids in the liquid-crystalline state with respect to the macroscopic bilayer normal. The order profiles for fluid-phase DHA and AA bilayers have the same general features at all temperatures studied. The segmental order parameters decrease with increasing temperature for both lipids, with the absolute magnitudes being lower for the AA bilayers.

Equilibrium Structural Parameters. Fluid-state structural parameters obtained from the plateau $S_{CD}^{(i)}$ values[29,42] are summarized in Table 1. We find that the cross-sectional area $\langle A_C \rangle$ of the saturated *sn*-1 chain is larger when esterified next to AA than next to DHA, with a corresponding reduction of the projection lengths $L_C^{*(n:0)}$ and $L_C^{(n:0)}$. Both areas are larger than the area per chain of the benchmark 14-carbon, disaturated lipid DMPC, designated in Table 1 as (14:0)(14:0)PC (also in the fluid state at these temperatures). We note that the structural parameters that we obtain from ^{2}H NMR in the case of mixed-chain bilayers correspond to partial contributions of the labeled saturated (16:0) *sn*-1 chain. The total lipid cross-sectional area and the net hydrocarbon thickness include the (unknown) contribution of the polyunsaturated *sn*-2 chains[29] (see below).

X-ray Diffraction Studies of ω-3 and ω-6 Polyunsaturated Bilayers. Direct measurements of global structural parameters were also obtained by small-angle X-ray diffraction. The X-ray diffraction patterns contained a broad wide-angle band corre-

Table 1. Structural Results for Lipids in the Liquid-Crystalline (L_α) State

T/°C	lipid	S_p[a]	D_C[b]/Å	$\langle A_C \rangle$[c]/Å^2	$L_C^{*(n:0)}$[d]	$L_C^{(n:0)}$[e]
15	(16:0)(20:4)PC	0.208	14.5	29.8	11.3	12.7
	(16:0)(22:6)PC	0.223	15.0	28.9	11.8	13.2
30	(14:0)(14:0)PC	0.213	12.8	30.0	10.6	12.2
	(16:0)(22:1)PC	0.225	15.0	29.3	12.5	14.0
	(16:0)(20:4)PC	0.191	14.0	31.5	10.8	12.1
	(16:0)(22:6)PC	0.204	14.4	30.6	11.2	12.5
50	(14:0)(14:0)PC	0.184	12.0	32.7	9.7	11.2
	(16:0)(16:0)PC	0.198	14.2	31.7	11.8	13.3
	(16:0)(22:1)PC	0.189	13.9	32.4	11.5	12.9
	(16:0)(22:6)PC	0.181	13.6	33.0	10.5	11.6

[a] Plateau order parameters used to calculate *sn*-1 saturated chain structural values. [b] Volumetric thickness (eq 14). [c] Cross-sectional area (eq 13). [d] Projection length (eq 15). [e] Projection length (eq 16).

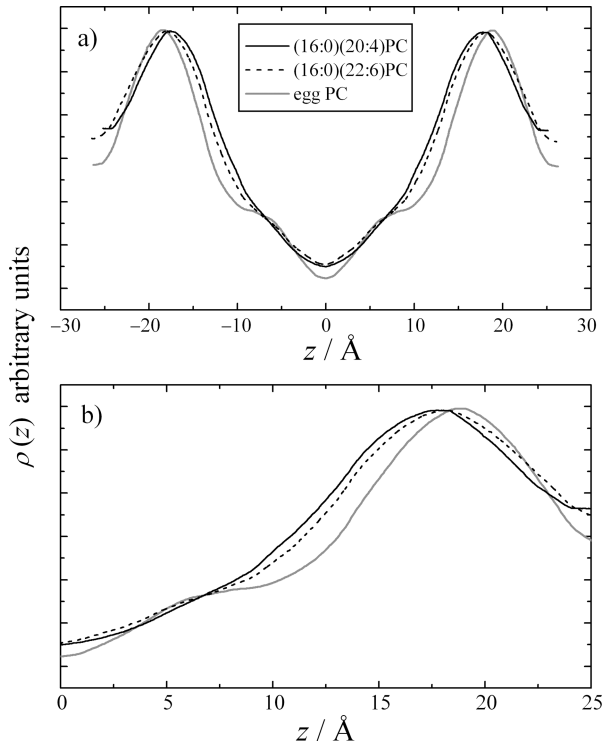

Figure 6. Comparison of electron density profiles of (16:0-d_{31})(20:4)PC and (16:0-d_{31})(22:6)PC with egg PC at 93% relative humidity and 20 °C. The profiles are plotted on a relative scale (arbitrary units) such that headgroup heights coincide. (a) Full electron density profiles along the bilayer normal direction and (b) expansion of electron density profiles across one-half the unit cell. The electron densities of (16:0-d_{31})(20:4)PC and (16:0-d_{31})(22:6)PC are similar, yet they differ from egg PC. The latter shows a larger bilayer thickness (headgroup separation) and a more ordered hydrocarbon region (more pronounced terminal methyl trough).

sponding to a lattice spacing of 4.5 Å and five sharp low-angle reflections, which indexed as orders of a lamellar repeat period (not shown). As indicated by the broad wide-angle band, the bilayers were in the liquid-crystalline state under these experimental conditions. The lamellar repeat period was 49 Å for the (16:0)(20:4)PC bilayer and 51 Å for (16:0)(22:6)PC. Electron density profiles for the AA and the DHA bilayers at 20 °C and 93% relative humidity are shown in Figure 6. They indicate that the difference in repeat period between (16:0)(20:4)PC and (16:0)(22:6)PC arises from a combination of a larger bilayer thickness and a larger fluid separation for (16:0)(22:6)PC.

Although the samples were only partially hydrated under these conditions, the structures should be directly comparable to fully hydrated bilayers.[33,46] The water content, estimated at about 15 waters per lipid, indicates that the bilayer deformations induced by dehydration are within an elastic regime.[47] Peaks in the electron density profiles in Figure 6 correspond to the electron-rich phosphocholine headgroups, and the low-density trough is due to the terminal methyl group in the center of the bilayer. The medium-density regions between the headgroup peaks and the terminal methyl trough represent the methylene acyl chain segments. Compared to egg phosphatidylcholine (egg PC), a well-studied mixture of saturated and monounsaturated phospholipids,[33,48] both polyunsaturated bilayers show a more disordered acyl chain region, as indicated by the broader features of the methyl troughs. This leads to thinner bilayers for DHA and AA bilayers than for egg PC. The measured head−head distances (D_{HH}) are 35.3 Å for (16:0)(20:4)PC and 35.7 Å for (16:0)(22:6)PC, compared to 37.2 Å for egg PC. Interestingly, the AA-containing bilayer is more disordered than the DHA bilayer, consistent with the ^{2}H NMR order parameters in Figure 5.

Using the values for D_{HH} from Figure 6, we can estimate the hydrocarbon thickness by subtracting the contribution from the PC headgroup. The width to be subtracted has been estimated at about 4.3 Å for phosphatidylcholine lipids.[47−49] In this way we obtain molecular hydrocarbon thicknesses of 13.4 Å, 13.6 Å, and 14.3 Å for (16:0)(20:4)PC, (16:0)(22:6)PC, and egg PC, respectively. The total bilayer hydrocarbon thicknesses are twice these values and are 26.8 Å for (16:0)(20:4)PC and 27.2 Å for (16:0)(22:6)PC. Thus, part of the observed difference in repeat period between (16:0)(20:4)PC and (16:0)(22:6)PC is due to a difference in bilayer hydrocarbon thickness, with the remainder due to a difference in interbilayer separation. These values compare well with previous estimates of D_C = 13.9 Å for (16:0-d_{31})(22:6)PC[29] and D_C = 14.2 Å for egg PC at 30 °C and 29 atm osmotic pressure.[33] We note that the net hydrocarbon thicknesses measured by X-ray diffraction can differ from the partial contributions of the saturated (16:0) *sn*-1 chain in Table 1, the main reason being chain-length mismatch at the bilayer center. In particular, for (16:0-d_{31})(22:6)PC at 30 °C, we have previously shown[29] that the net volumetric thickness D_C is 13.9 Å, while the *sn*-1 partial thickness $D_C^{(16:0)}$ = 14.4 Å, consistent with the current results.

Deuterium NMR Relaxation and Membrane Dynamics. Next, ^{2}H spin−lattice relaxation rates, R_{1Z}, were measured for both the DHA and AA bilayers using the inversion recovery method. In Figure 7, we show a representative relaxation sequence for (16:0-d_{31})(20:4)PC, with random (powder-type) and de-Paked ^{2}H NMR spectra given in parts a and b, respectively. Recovery of each individual peak (resonance) is monitored most readily using the de-Paked spectral results; it is noteworthy that the rate of inversion recovery increases as the residual quadrupolar couplings become greater. The larger splittings corresponding to the plateau region revert in less than 15 ms and fully recover after 40−50 ms. By contrast, the inner splittings take much longer; in particular the methyl resonance in Figure 7 is still inverted at 110 ms.

(46) Koenig, B. W.; Strey, H. H.; Gawrisch, K. *Biophys. J.* **1997**, *73*, 1954−1966.
(47) Nagle, J. F.; Tristram-Nagle, S. *Biochim. Biophys. Acta* **2000**, *1469*, 159−195.
(48) McIntosh, T. J.; Simon, S. A. *Biochemistry* **1986**, *25*, 4058−4066.
(49) Sachs, J. N.; Petrache, H. I.; Woolf, T. B. *Chem. Phys. Lipids* **2003**, *126*, 211−223.

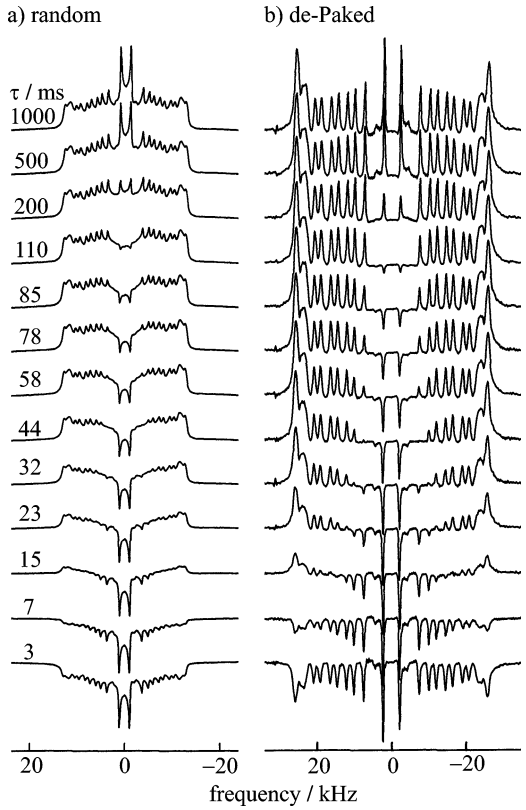

Figure 7. Representative partially relaxed ^{2}H NMR spectra of randomly oriented multilamellar dispersions of (16:0-d_{31})(20:4)PC containing 50 wt % H_2O in the L_α phase at 15 °C. (a) Powder-type spectra and (b) corresponding de-Paked spectra. Values of the delay τ between the inverting and quadrupolar-echo pulse elements are indicated.

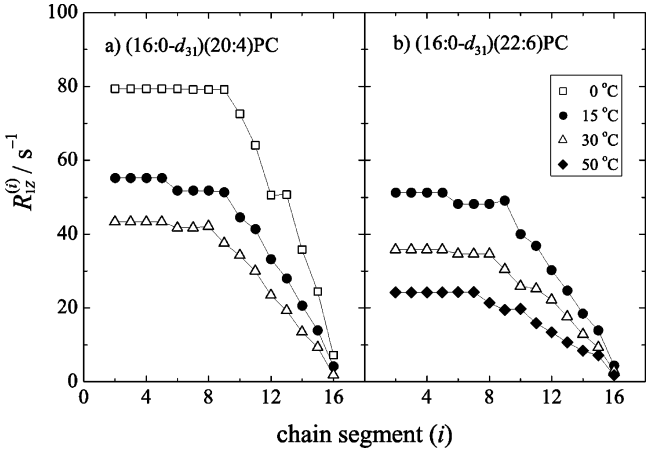

Figure 8. Profiles of spin−lattice (Zeeman) relaxation rates $R_{1Z}^{(i)}$ as a function of *sn*-1 acyl segment position for (a) (16:0-d_{31})(20:4)PC and (b) (16:0-d_{31})(22:6)PC in the L_α phase at various temperatures. For both lipids, the relaxation rates decrease with increasing temperature. At a given absolute temperature, the relaxation rates for (16:0-d_{31})(20:4)PC are *larger* than those for (16:0-d_{31})(22:6)PC.

For each of the resonances, the recovery process is exponential in time and is characterized by a decay (rate) parameter, R_{1Z}, the spin−lattice (Zeeman) relaxation rate. The rate values, determined for all well-resolved peaks, are plotted in Figure 8 as a function of the chain segment index *i*. The relaxation rates decrease along the acyl chain, in striking resemblance to the order parameter profiles. There is also a strong temperature variation, with smaller rates at larger temperatures, similar again to the order parameter behavior (cf. Figure 5). In terms

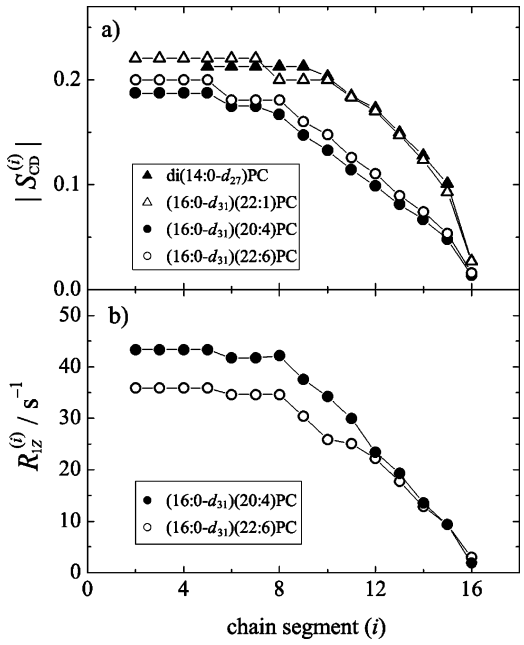

Figure 9. Comparison of (a) order parameter profiles and (b) relaxation rate profiles for (16:0-d_{31})(20:4)PC and (16:0-d_{31})(22:6)PC bilayers at 30 °C. Part a also shows data for di(14:0-d_{27})PC[41] and (16:0-d_{31})(22:1)PC for contrast with disaturated and monounsaturated lipid bilayers. The indexing of the 14:0-d_{27} carbon segments has been shifted to the right to coincide at the ω carbon (see text.) The order parameters of polyunsaturated bilayers are quite similar, while differing markedly from the disaturated and monounsaturated profiles. By contrast, the relaxation profiles in part b differ significantly between the ω-3 and the ω-6 bilayers.

of relaxation times, $T_{1Z} = 1/R_{1Z}$, the plateau segments of AA bilayers recover twice as fast at 15 °C than at 30 °C, specifically 12.5 ms versus 22.7 ms. The slower terminal methyl groups have relaxation times varying from 140 ms at 15 °C to 520 ms at 30 °C.

In Figure 9, profiles of the order parameters and relaxation rates are compared at 30 °C. In part a, we also include order parameters for the disaturated di(14:0-d_{27})PC[42] and the monounsaturated (16:0-d_{31})(22:1)PC bilayers to emphasize the qualitatively different chain packing of polyunsaturated lipids. While the profiles of the disaturated and monounsaturated bilayers show a pronounced curvature, the variation along the chain is more gradual in the case of mixed-chain saturated−polyunsaturated bilayers.[25,29] We have recently interpreted this difference in terms of a universal, continuous chain packing profile of saturated acyl chains. Following ref 29, the DMPC profile in Figure 9a is shifted by two carbon positions to enable comparison with the 16:0 profile of the monounsaturated (16:0-d_{31})(22:1)PC bilayer. There is practically no difference between these two profiles in the core of the hydrocarbon region (nonplateau carbon segments). However, in the presence of a polyunsaturated chain at position *sn*-2, a dramatic change of the order parameter profile is seen. The order parameters for the saturated (16:0) chain are altered substantially if either the AA or the DHA polyunsaturated chain is esterified at position *sn*-2, with only slight variations between the AA and DHA bilayers. Interestingly, the relaxation rates of AA and DHA bilayers shown in Figure 9b differ appreciably. There are lower relaxation rates for the DHA bilayer than for the AA bilayer, with pronounced differences in the plateau region of the saturated *sn*-1 chain. Dissimilar relaxation rates are also found for lipids containing another member of the ω-6 class, docosa-

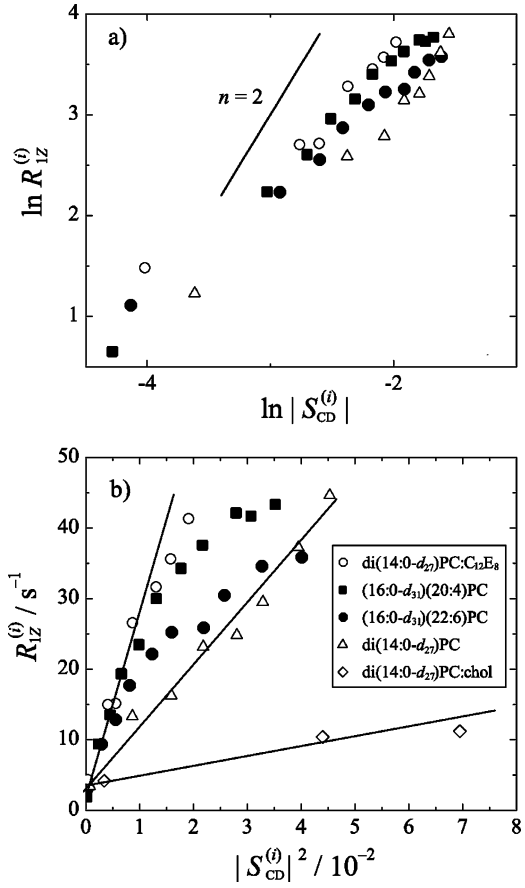

Figure 10. Functional dependence of relaxation rate $R_{1Z}^{(i)}$ and order parameter $S_{CD}^{(i)}$ profiles at 30 °C. (a) Logarithmic plots of relaxation rate dependence on order parameters. Data for the polyunsaturated (16:0-d_{31})-(20:4)PC and (16:0-d_{31})(22:6)PC bilayers are compared to those for the disaturated DMPC-d_{54} bilayer[41] and its 2:1 mixture with the nonionic detergent $C_{18}E_8$.[49] The slope of $n = 2$ expected for a square-law dependence of R_{1Z} on S_{CD} in the absence of a constant contribution is indicated for reference. (b) Square-law dependence of $R_{1Z}^{(i)}$ and $|S_{CD}^{(i)}|$ for the data in part a also including a DMPC-d_{54}/cholesterol (1:1) mixture.[52] The overall slope of the $R_{1Z}^{(i)}$ versus $|S_{CD}^{(i)}|^2$ curves is a measure of bilayer softness with a larger slope indicating greater deformability.

pentaenoic acid (22:5ω-6)[2], having the same number of carbons as DHA but with one less double bond.

At this juncture the question naturally arises as to how we should contrast the relaxation rates of AA and DHA bilayers with those of saturated and monounsaturated bilayers. For instance, how does one evaluate relaxation rates when the amplitudes of motions differ? The practical solution is to bypass the chain indexing and look directly at correlations between relaxation and order parameters.[50] (Elsewhere we have shown[29,42] that conventional chain indexing is actually not the most convenient basis for comparing bilayers, as it can obscure universal laws governing acyl-chain packing.) Therefore, logarithmic plots of relaxation data versus order parameters are shown in Figure 10a. Here the relaxation rates for the different bilayers are compared at the same amplitude of motion, i.e., order parameter value[50] in a model-free way. We also show results for di(14:0-d_{27})PC with and without a nonionic detergent ($C_{18}E_8$) to provide reference values for the measured rates.[51] Experimentally, the R_{1Z} rates for a given value of the order parameter S_{CD} increase from DMPC to (16:0)(22:6)PC, to (16:0)(20:4), and finally to the DMPC/$C_{18}E_8$ mixture. Given that detergent additives soften the lipid bilayers, an upward shift of data points in Figure 10a indicates softer (less rigid) bilayers. By this measure, AA-containing bilayers are softer than those containing DHA.

The results in Figure 10a imply that there is a functional dependence of the R_{1Z} relaxation rates on the motional amplitudes as described by the segmental order parameter S_{CD}, for otherwise the data would be randomly distributed. The power law dependence of R_{1Z} on S_{CD} is close to the value of 2 expected if the relaxation is governed by fluctuations in the local order parameters of the acyl chain segments due to motion of the whole bilayer. In such a case, Fermi's Golden Rule implies that the mean-square amplitudes of local motions are proportional to the order parameters, which are modulated by nearly the same type of slow motion regardless of depth within the bilayer. Examples of such relatively slow motions are noncollective molecular rotations or collective excitations of the bilayer lipids.

Within such a framework,[50] the plots of R_{1Z} versus $|S_{CD}|^2$ shown in Figure 10b are semiempirical estimates of bilayer softness (viscoelasticity). The experimental relationship between the mobility as given by the R_{1Z} rate and the motional amplitude as given by $|S_{CD}|^2$ provides us with a practical way of comparing lipid bilayers in terms of their viscoelastic properties. Calibration lines are provided by the benchmark DMPC bilayer[50] and its softer and stiffer mixtures with detergent[51] and cholesterol,[52] respectively. A steeper slope in Figure 10b reflects a softer, more flexible bilayer. In counterclockwise direction, the calibration lines correspond to bending rigidities, κ, of approximately $100k_BT$, $11k_BT$, and $6k_BT$.[50] Our results show that the mixed-chain saturated−polyunsaturated bilayers have bending rigidities between 6 and $11k_BT$, with the arachidonic bilayers being notably softer than the DHA bilayers.

Discussion

Polyunsaturated phospholipids of the ω-3 and ω-6 families play key biological roles; however their functional mechanisms remain unclear. While the ω-6 arachidonic acid acts as second messenger, nonspecific functions of the ω-3 class are suggested by their high content in neuronal and retinal membranes, as well as spermatozoa. By applying deuterium NMR spectroscopy and small-angle X-ray diffraction, we discovered that polyunsaturated lipids form markedly different bilayers as compared to saturated and even monounsaturated lipids. At physiological temperatures, polyunsaturated bilayers are in the fluid phase, with disordered acyl chains commonly assumed to be the biologically relevant state of lipids.[25,31] They form highly ordered states at lower temperatures,[31,53] referred to as gel phase, which are usually considered much too rigid for biological functions. To understand the molecular organization of polyunsaturated lipids (cf. Figure 1), it is necessary to document the bilayer properties both below and above the chain melting

(50) (a) Brown, M. F.; Thurmond, R. L.; Dodd, S. W.; Otten, D.; Beyer, K. *Phys. Rev. E* **2001**, *64*, 010901/1−010901/4. (b) Brown, M. F.; Thurmond, R. L.; Dodd, S. W.; Otten, D.; Beyer, K. *J. Am. Chem. Soc.* **2002**, *124*, 8471−8484. (c) Martinez, G. V.; Dykstra, E. M.; Lope-Piedrafita, S.; Job, C.; Brown, M. F. *Phys. Rev. E* **2002**, *66*, 050902/1−050902/4. (d) Martinez, G. V.; Dykstra, E. M.; Lope-Piedrafita, S.; Brown, M. F. *Langmuir* **2004**, *20*, 1043−1046.

(51) Otten, D.; Brown, M. F.; Beyer, K. *J. Phys. Chem. B* **2000**, *104*, 12119−12129.

(52) Trouard, T. P.; Nevzorov, A. A.; Alam, T. M.; Job, C.; Zajicek, J.; Brown, M. F. *J. Chem. Phys.* **1999**, *110*, 8802−8818.

(53) Applegate, K. R.; Glomset, J. A. *J. Lipid Res.* **1986**, *27*, 658−680.

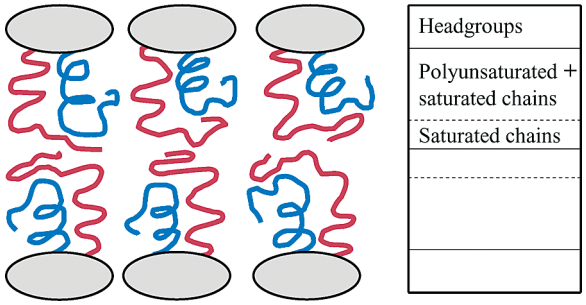

Figure 11. Schematic representation of the acyl chain mass distribution for mixed-chain saturated−polyunsaturated phosphatidylcholines in the fluid (L_α) state. The saturated chain (red) is displaced toward the bilayer center, while the polyunsaturated chain (blue) is located closer to the water interface. This mass shift can generate distinct bending moments for polyunsaturated bilayers compared to disaturated bilayers.

transition, where marked changes in the acyl chain packing occur. Structural and dynamical differences are evident in both the ordered and disordered, liquid-crystalline phases. In particular, we find that polyunsaturated bilayers in the fluid state are thinner, with a larger interfacial area, and more flexible than the corresponding saturated and monounsaturated bilayers. Another interesting feature of mixed saturated−polyunsaturated bilayers is that the PUFA chains are displaced toward the aqueous interface relative to the saturated chains.[29]

Dynamical Structure of Polyunsaturated Phospholipid Bilayers. In applications of solid-state ^{2}H NMR spectroscopy to biomolecular systems there are two kinds of observables. As described above, the order parameters are indicative of equilibrium properties, whereas the relaxation parameters characterize the dynamics.[37] The relationship between these quantities tells us about the types of molecular motions within the bilayer. Because ^{2}H NMR spectroscopy provides knowledge of the order and mobility of C−^{2}H segments, it has been applied to study the influences of monounsaturation and polyunsaturation on the structure and dynamics of phospholipid bilayers.[1,2,25,29−32,54] In this regard, a clear distinction can be made based on the dramatic alterations of the order profile shapes of the saturated *sn*-1 chain in the presence of polyunsaturated acyl groups. An important aspect, as we have shown previously, is that disaturated lipids with various chain lengths (forming a homologous series) trace a universal chain packing profile.[42] For each bilayer, this universal packing profile is sampled discretely according to the acyl chain length.[29] The only difference is the increased order and extension of the plateau region for the longer chains. By contrast, little or no change of order is evident near the bilayer center with increasing acyl chain length. We therefore speak of a neutral volume at the bilayer center, invariant to chain substitutions involving saturated and monounsaturated chains.[29]

However, an interesting shift of this neutral region occurs when a polyunsaturated chain is esterified at position *sn*-2. For PUFA-containing bilayers, more disordered states for the saturated *sn*-1 chain become available due to shifting of its mass toward the bilayer center,[29] as shown schematically in Figure 11. The displacement of the *sn*-1 saturated group is accompanied by a concomitant shift in mass of the *sn*-2 PUFA chain in the direction of the lipid/water interface, which can be related to the conformational flexibility of the polyunsaturated acyl group.[29] This uneven mass distribution can result in different bending moments for the polyunsaturated bilayers compared to disaturated bilayers. For instance, the lateral pressure profile across the bilayer[55,56] could be affected, or, equivalently, the spontaneous curvature,[55,57] which may in turn influence the conformational energetics of membrane proteins.[24,26,27]

Orientational Ordering and Average Structure of Bilayers of ω-3 and ω-6 Phospholipids. In the present work, the saturated chain at the glycerol *sn*-1 position reflects the interactions with the polyunsaturated fatty acyl group esterified at the *sn*-2 position, as evidenced by the ^{2}H NMR spectra and the corresponding order profiles. For the gel phase, the smooth decrease of intensity from the center to the edges of the ^{2}H NMR spectra of DHA bilayers, compared to that in AA bilayers (cf. Figure 2), indicates a broader distribution of splittings in the former, revealing different order gradients along the chains. However, in the liquid-crystalline (L_α) phase, the $S_{CD}^{(i)}$ values of all segments of the *sn*-1 palmitoyl chain are larger when esterified next to a DHA chain than when adjacent to an AA chain. By this measure, the DHA bilayer in the L_α phase is more ordered than the AA bilayer. We suggest that this tendency of the DHA bilayer to form more ordered structures than the AA bilayer could be manifested in lipid mixtures under biological conditions and could possibly influence the activity of membrane-bound proteins, such as phospholipase A_2.[15]

Further interpretation of the order profiles requires the introduction of motional models such as those based on mean-field theories.[58] Here we have estimated average structural parameters of the *sn*-1 acyl chains using a first-order mean-torque model.[41,42] Compared to less unsaturated phospholipids with similar acyl lengths, the polyunsaturated bilayers are thinner and have a correspondingly larger interfacial area per lipid molecule. Notably, similar increases in the area per molecule for AA and DHA bilayers compared to monounsaturated lipids have also been measured in monolayers at the air/water interface at a constant applied pressure.[59] Moreover, in the fluid L_α state at the same absolute temperature, we find a larger *sn*-1 chain cross-sectional area for AA bilayers than for DHA bilayers. This is a result of increased disorder in the former, as shown by the partial cross-sectional areas A_C and the corresponding volumetric thicknesses D_C. In consequence, the shorter AA chain makes the bilayer more disordered; it is thinner with a larger cross-sectional area than that of DHA bilayers (see below).

X-ray measurements on partially dehydrated multilayers in the fluid L_α state also substantiate the above conclusions drawn from solid-state ^{2}H NMR spectroscopy. It is noteworthy that the electron density profiles of both AA and DHA bilayers are

(54) (a) Deese, A. J.; Dratz, E. A.; Dahlquist, F. W.; Paddy, M. R. *Biochemistry* **1981**, *20*, 6420−6427. (b) Paddy, M. R.; Dahlquist, F. W.; Dratz, E. A.; Deese, A. J. *Biochemistry* **1985**, *24*, 5988−5995. (c) Huster, D.; Arnold, K.; Gawrisch, K. *Biochemistry* **1998**, *37*, 17299−17308. (d) Binder, H.; Gawrsich, K. *Biophys. J.* **2001**, *81*, 969−982. (e) Brzustowicz, M. R.; Cherezov, V.; Caffrey, M.; Stillwell, W.; Wassall, S. R. *Biophys. J.* **2002**, *82*, 285−298. (f) Shaikh, S. R.; Brzustowicz, M. R.; Gustafson, N.; Stillwell, W.; Wassall, S. R. *Biochemistry* **2002**, *41*, 10593−10602. (g) Brzustowicz, M. R.; Cherezov, V.; Zeruga, M.; Caffrey, M.; Stillwell, W.; Wassall, S. R. *Biochemistry* **2002**, *41*, 12509−12519. (h) Shaikh, S. R.; Dumaual, A. C.; Castillo, A.; LoCascio, D.; Siddiqui, R. A.; Stillwell, W.; Wassall, S. R. *Biophys. J.* **2004**, *87*, 1752−1766. (i) Wassall, S. R.; Brzustowicz, M. R.; Shaikh, S. R.; Cherezov, V.; Caffrey, M.; Stillwell, W. *Chem. Phys. Lipids* **2004**, *132*, 79−88.
(55) Brown, M. F. *Chem. Phys. Lipids* **1994**, *74*, 159−180.
(56) Cantor, R. S. *Biophys. J.* **1999**, *76*, 2625−2639.
(57) (a) Gruner, S. M. *J. Phys. Chem.* **1989**, *93*, 7562−7570. (b) Seddon, J. M. *Biochim. Biophys. Acta* **1990**, *1031*, 1−69.
(58) (a) Marčelja, S. *Biochim. Biophys. Acta* **1974**, *367*, 165−176. (b) Meraldi, J.-P.; Schlitter, J. *Biochim. Biophys. Acta* **1981**, *645*, 183−192. (c) Meraldi, J.-P.; Schlitter, J. *Biochim. Biophys. Acta* **1981**, *645*, 193−210.
(59) Brockman, H. L.; Applegate, K. R.; Momsen, M. M.; King, W. C.; Glomset, J. A. *Biophys. J.* **2003**, *85*, 2384−2396.

quite distinct from that of egg PC, which has a lower density trough in the center of the bilayer and a significantly larger peak-to-peak distance. The electron density profiles obtained from X-ray data indicate that the bilayer thickness, as measured by the peak-to-peak distance, is smaller for the AA bilayer than for the DHA bilayer. Thus a consistent picture is reached from consideration of both ^{2}H NMR and small-angle X-ray diffraction data.

Comparison to Quantum Mechanical Calculations and Molecular Mechanics Simulations. The conformational flexibility of the polyunsaturated chains in fluid-state bilayers has been theoretically investigated by means of molecular dynamics simulations.[2,60,61] An important observation is that polyallylic triene sequences can form helical and iron-angle conformations, previously described[53] in the case of energy minimized structures. At higher temperatures, the correlations between such triene segments are reduced due to the low potential energy barriers,[2,60,61] generating back-bent (upturn or hairpin) conformations which increase the cross-sectional area per lipid. Simulations also indicate that the average center of mass of the PUFA chains is shifted by an increased contribution from back-bended or hairpinlike conformers, arising from the repeating $-CH{=}CH-CH_2-$ polyallylic motif.[2,60,61]

Further differences in the conformational flexibility of PUFAs relative to less unsaturated acyl chains are suggested by ab initio quantum mechanical calculations.[60,62] These results are included in classical molecular mechanics simulations of DHA-phospholipid bilayers and AA-phospholipid bilayers.[63] Here these studies reveal substantially lower potential energy barriers to rotational isomerizations. For polyunsaturated acyl chains, the rotational isomerization of the doubly allylic $CH{=}CH-CH_2-CH{=}CH$ groups is from skew$^{\pm}$ to skew,$^{\mp}$ as compared to the trans to gauche$^{\pm}$ isomerizations of saturated chains. Within the context of activated complex theory, this finding might suggest a greater rate of rotational isomerization of PUFA chains.[2] On the other hand, in condensed media such as lipid bilayers, the diffusion-limited regime for segmental motions of the acyl groups may be applicable. In accord with this picture, the rates of segmental motions may be governed by the effective membrane viscosity, together with the hydrodynamic volume of the acyl segment undergoing reorientation.[64]

Thermotropic Behavior of Mixed-Chain Polyunsaturated Phospholipid Bilayers. One marked difference between the ω-3 and ω-6 bilayers involves their thermotropic behavior. Due to the presence of double bonds, both the AA and DHA lipids melt at significantly lower temperatures than disaturated lipids. Cooperativity and hysteresis of the order−disorder transitions of mixed-chain DHA-phospholipid bilayers have been demonstrated previously.[31] The degree of hysteresis was found to decrease systematically with the length of the *sn*-1 saturated chain (reduced acyl carbon mismatch) and was almost negligible for the (18:0-d_{31})(22:6)PC bilayer.[2,31] As a result, one can infer that the 18:0 and 22:6 chains are matched; i.e., the polymethylene and polyallylic acyl groups have similar lengths projected along the bilayer normal in the low-temperature gel state. In addition, the hysteresis depends on the position of the double bonds, as a similar distinction has been reported between the isomeric linolenic lipids (16:0-d_{31})(α18:3)PC and (16:0-d_{31})(γ18:3)PC.[45] It is interesting that the phase transition temperature of the (16:0-d_{31})(20:4)PC bilayer is significantly less than that of (16:0-d_{31})(22:6)PC, despite its lower degree of unsaturation. Clearly, the phase transition temperature depends not only on the number and position of the double bonds, but also on the length of the polyunsaturated acyl chain.[31,65] The melting temperatures for the ω-3 lipid (18:0-d_{31})(22:6)PC and the ω-6 lipid (18:0-d_{31})(22:5)PC, both with 22 carbons at position *sn*-2, have been shown to be practically the same despite the loss of a double bond in the latter case.[2] We therefore conclude that the reason the DHA bilayer melts at a higher temperature than the AA bilayer is the longer PUFA chain length. The increased length of the DHA chain apparently overcomes the effect of increased unsaturation.

In the present work, both the sharpness and hysteresis of the phase transition in DHA bilayers suggest a higher degree of cooperativity among the phospholipid acyl chains as compared to the AA bilayers. As noted above, the conformational preferences could be influenced by the length match of the polyunsaturated and saturated acyl chains in the mixed-chain phospholipid bilayers. For a lesser degree of matching of the PUFA and saturated chains, as may be the case for the AA bilayer, a reduction of the melting point and broadening might occur. The large hysteresis of the DHA bilayer may be due to a substantially increased propensity to form angle-iron conformers in the gel state and back-bended, hairpin-like conformers in the fluid state, e.g., involving the ultimate CH═CH group of the chain, as suggested by molecular dynamics studies.[60] The conformational changes can occur with a high degree of cooperativity for the DHA bilayer, as mentioned above. Such back-bended conformers could also be associated with the report of a greater lateral compressibility of DHA-phospholipid bilayers (lower area compressibility modulus K_A) versus monounsaturated phospholipid bilayers.[46]

Structural Dynamics of Polyunsaturated Phospholipid Bilayers. Turning next to the dynamical properties of phospholipid bilayers, we know that ^{2}H nuclear spin relaxation studies are a valuable source of information. An important issue involves disentangling the relative contributions from the various types of motions to the structural dynamics in the fluid state.[37] These include (i) local segmental motions of the flexible lipids, due to the internal chain dynamics, as well as (ii) slower motions formulated either as molecular rotational diffusion within the mean-torque potential of the bilayer,[66,67] or alternately collective membrane deformations.[66,68] Studies of the dependence of the relaxation rates on frequency, temperature, and the degree of bilayer order are valuable in this regard.[66,68] Moreover, by considering the dependence of the relaxation on the orientational

(60) Huber, T.; Rajamoorthi, K.; Kurze, V. F.; Beyer, K.; Brown, M. F. *J. Am. Chem. Soc.* **2001**, *124*, 298−309.
(61) (a) Saiz, L.; Klein, M. L. *J. Am. Chem. Soc.*, **2001**, *123*, 7381−7387. (b) Saiz, L.; Klein, M. L. *Biophys. J.* **2001**, *81*, 204−216.
(62) Feller, S. E.; Gawrisch, K.; MacKerell, A. D. *J. Am. Chem. Soc.* **2002**, *124*, 318−326.
(63) Rich, M. R. *Biochim. Biophys. Acta* **1993**, *1178*, 87−96.
(64) Brown, M. F.; Seelig, J.; Häberlen, U. *J. Chem. Phys.* **1979**, *70*, 5045−5053.
(65) Koynova, R.; Caffrey, M. *Biochim. Biophys. Acta* **1998**, *1376*, 91−145.
(66) Brown, M. F. *J. Chem. Phys.* **1982**, *77*, 1576−1599.
(67) (a) Rommel, E.; Noack, F.; Meier, P.; Kothe, G. *J. Phys. Chem.* **1988**, *92*, 2981−2987. (b) Halle, B. *J. Phys. Chem.* **1991**, *95*, 6724−6733.
(68) (a) Brown, M. F.; Ribeiro, A. A.; Williams, G. D. *Proc. Natl. Acad. Sci. U.S.A.* **1983**, *80*, 4325−4329. (b) Brown, M. F. *J. Chem. Phys.* **1984**, *80*, 2808−2831. (c) Brown, M. F.; Söderman, O. *Chem. Phys. Lett.* **1990**, *167*, 158−164. (d) Nevzorov, A. A.; Brown, M. F. *J. Chem. Phys.* **1997**, *107*, 10288−10310. (e) Nevzorov, A. A.; Trouard, T. P.; Brown, M. F. *Phys. Rev. E* **1998**, *58*, 2259−2281.

order of the acyl segments at a single resonance frequency, it is possible to utilize more detailed studies of model lipids[68] as a framework for acquiring further knowledge of the properties of lipid bilayers in the fluid (L_α) state.

Let us first consider the contribution from local segmental motions of the acyl groups within the bilayer hydrocarbon region. In the case of unsaturated lipid bilayers, the CH═CH groups have a larger volume than the CH_2 groups of saturated chains. For a diffusion-like picture, local motions of unsaturated chains are therefore expected to be more sluggish. Indeed, ^{2}H NMR and ^{13}C NMR relaxation studies of unsaturated and polyunsaturated lipid bilayers suggest that the local motions of the CH═CH groups of unsaturated bilayers are slower; i.e., the correlation times are longer than for the CH_2 groups of saturated bilayers.[64,69] It follows that the contribution from the internal chain dynamics to the NMR relaxation of the CH═CH groups of polyunsaturated bilayers may be greater than that for the CH_2 groups. The repeating polyallylic motif of −CH═CH−CH_2− groups of the polyunsaturated acyl chains would then imply that the internal dynamics of the entire acyl chain could be slower than in the case of less unsaturated bilayers. It is also noteworthy that the apparent activation energies (E_a) obtained experimentally from analysis of the ^{13}C R_{1Z} rates of polyunsaturated lipid bilayers are larger than the quantum mechanical or molecular dynamics potential barriers for segmental isomerization. Even in the case of polyunsaturated lipid bilayers,[69] the E_a values are approximately the same or larger than for monounsaturated and saturated bilayers.[64] One can conclude that the motions which govern the relaxation of polyunsaturated bilayer lipids are most likely not in the activation-controlled limit for rotational isomerization[2] but rather depend on diffusive motions within the effective viscosity of the membrane hydrocarbon region.[64,66]

For fluid bilayers, the dynamics of the lipids may encompass significant contributions from collective motions of the bilayer aggregate,[66,68] in addition to the local motions. The observed NMR relaxation rates are then determined by the composite or resultant (effective) motions of the lipids.[66] Within a continuum description, the contribution of collective motions depends on material properties of lipid bilayers, for example, the bilayer softness or deformability of the membrane over relatively short length scales. This means that despite the sluggish local (internal) motions of the *sn*-2 polyunsaturated acyl chains, the composite motions of the lipids as manifested by the *sn*-1 saturated chains could still be relatively fast if the bilayers are soft with respect to quasi-elastic deformations. Although the assumption of time-scale separation may break down due to convergence of the relatively fast and slow motions, there is nonetheless experimental evidence that such a simplified view is useful in interpreting the NMR relaxation of fluid bilayers.[50]

Viscoelastic Properties of ω-3 and ω-6 Polyunsaturated Bilayers on Mesoscopic Length Scales Deduced from Nuclear Spin Relaxation. In this article we consider melted chains by correlating the relaxation with the orientational order parameters, the two NMR observables. When evaluated at the same amplitude of motion, relaxation parameters provide a naturally calibrated scale for comparison of lipid bilayers.[50,66] Reference data are provided by benchmark disaturated phospholipids and their mixtures with cholesterol and a nonionic detergent, whose viscoelastic properties are well investigated. We thus have found significant differences in the viscoelasticity of the ω-3 and ω-6 bilayers over short length scales approaching the molecular dimensions, which to a certain extent is an unforeseen observation that sets apart the two fatty acid types. In this context, one can consider a membrane deformation model which assumes two kinds of motions for the relaxation mechanism. The segmental motions are fast relative to the resonance frequency, and the ordering represents a small correction.[64] By contrast, the slow motions are due to collective fluctuations of the lipids, which modulate the residual quadrupolar coupling left over from the fast motions and depend on the square of the local order parameter.[66−68] If relatively slow motions are the major contribution to relaxation, an approximately linear dependence of R_{1Z} and $|S_{CD}|^2$ is expected. Such behavior is in fact observed for disaturated PCs in the fluid phase.[39,66] In terms of a square-law relation of the spin−lattice relaxation rate R_{1Z} and the order parameter S_{CD}, a steeper slope reflects a softer, more deformable bilayer. This is a measurable property which governs the response of the biological membrane material to physical perturbations, for example, due to interactions with cholesterol, detergents, and membrane proteins.

In the case of mixed-chain polyunsaturated bilayers, however, the square-law plots tend to depart from linearity, as implied by a simple composite deformation model. Such deviations are also observed for disaturated PCs at elevated temperatures,[70] where greater disorder in the chain leads to a relatively short plateau in the order profile. For both the (16:0-d_{31})(20:4)PC and (16:0-d_{31})(22:6)PC bilayers, the R_{1Z} values vary almost linearly with $|S_{CD}|^2$ from the methyl terminus up to about middle of the 16:0 acyl chain, with a downward curvature for the top part of the acyl chain. One should note that a square-law dependence requires that several assumptions be satisfied.[50] Included among these are: (i) time scale separation of the relatively fast motions of smaller amplitude from the slower motions of greater amplitude; (ii) a constant orientation and asymmetry parameter of the residual coupling tensor modulated by the motions; and (iii) a uniform amplitude of the relatively slow motions within the bilayer hydrocarbon region. It is not surprising that in the case of mixed-chain polyunsaturated bilayers some of these assumptions may break down.

Above, we have described how the ^{2}H NMR order profiles and the chain packing curves can be interpreted in terms of the acyl mass distributions, where the saturated *sn*-1 chain is displaced into the central bilayer region relative to the PUFA *sn*-2 chain, which is shifted toward the bilayer aqueous interface. The apparent curvature of R_{1Z} versus $|S_{CD}|^2$ in the fluid state might in fact reflect mismatch of the acyl chains in the mixed-chain bilayers. As a consequence of this chain packing, the lower part of the saturated acyl group would be in a more mobile or softer region of the bilayer, whereas the top part would strongly interact with the PUFA chain and would be less flexible. Moreover, the reduction in flexibility would be greater for ω-3 PUFAs such as DHA compared to ω-6 PUFAs such as AA, as seen experimentally. In line with this interpretation, for mixed-chain polyunsaturated bilayers one expects the square-law to be almost linear when the projected *sn*-1 saturated acyl length

(69) Zajicek, J.; Ellena, J. F.; Williams, J. D.; Khadim, M. A.; Brown, M. F. *Collect. Czech. Chem. Commun.* **1995**, *60*, 719−735.

(70) Dodd, S. W. M.S. Thesis, 1987, University of Virginia.

matches that of the *sn*-2 PUFA chain, with increasing deviation from linearity for greater acyl length mismatch.

Analysis of the correlation between the R_{1Z} rates and S_{CD} order parameters using a collective membrane deformation model indeed suggests that the polyunsaturated bilayers tend to be softer and more susceptible to elastic deformation on the mesoscopic length scale than their more saturated counterparts, at least in the central bilayer region. According to the classical theory of elasticity, such a reduction of the Helfrich bending elastic modulus κ[71] would in turn imply a concomitant reduction in K_A, the elastic modulus for interfacial area deformation. This reduction in K_A is consistent with the report of an increase in compressibility for DHA-phospholipid bilayers.[46] Even if the effective bilayer viscosity is similar to less unsaturated lipids, the composite motions of the polyunsaturated phospholipids could still be faster, due to a decrease in the bending rigidity associated with the dynamical softness of the membrane aggregate.

We have also shown an increased deformability of ω-6 arachidonic chains compared to ω-3 docosahexaenoic chains. Despite the small reduction in the order parameters, the spin−lattice relaxation rates of AA-containing bilayers are significantly larger than those containing DHA, emphasizing the importance of conducting both types of ^{2}H NMR measurements. Given this framework, there is an enhancement of the relaxation rate for a given value of the segmental order parameter; the ω-6 AA-phospholipid bilayer is softer and more deformable than the ω-3 DHA bilayer. This interpretation is consistent with weaker interactions of the AA chain with the saturated 16:0 *sn*-1 chain, giving rise to more disorder (larger amplitude of motion) and a lower order−disorder phase transition temperature (T_m) than in the presence of DHA. One interesting possibility is that an increased deformability of AA-phospholipid bilayers might be related to the fatty acid selectivity of phospholipase A_2 enzymes.[15]

Conclusions Regarding Differences in Biophysical Properties of Bilayers of ω-6 and ω-3 Phospholipids. The above findings reveal distinct differences in the structural dynamics of ω-3 versus ω-6 polyunsaturated lipid bilayers, apart from their dissimilarities relative to less unsaturated lipids. Our results suggest that the number and location of double bonds as well as acyl length differences affect the packing in mixed-chain lipid bilayers and should be taken into account when interpreting the physicochemical properties of biological membranes. Compared to bilayers of disaturated and monounsaturated phospholipids, there is an increased disorder of the saturated *sn*-1 chains in mixed chain, ω-3 and ω-6 polyunsaturated bilayers. The role of highly unsaturated fatty acids in biological membranes might be to support the function of certain membrane proteins that require low interfacial headgroup density, i.e., large cross-sectional lipid areas. Moreover the ω-6 AA bilayer is more disordered at the same absolute temperature; it is thinner and has a larger area per lipid compared to the ω-3 DHA-bilayer. By contrast, relaxation measurements show an opposite increase in the spin−lattice (R_{1Z}) relaxation rates of the *sn*-1 saturated chains due to the presence of ω-6 arachidonic chains compared to ω-3 docosahexaenoic chains in mixed-chain bilayers. Adopting a simple membrane deformation model we find that the ω-6 AA-phospholipid bilayer appears to be softer and more deformable than the ω-3 DHA bilayer. This interpretation constitutes an unanticipated and perhaps biologically meaningful result that distinguishes between the two fatty acid types. One possibility is that variations in deformability of AA and DHA-phospholiplid bilayers might be related to the fatty acid preference of various enzymes. The additional significance of these findings is that chemically nonspecific influences of bilayer lipids may govern their coupling to membrane proteins linked to key biological functions, as in the case of rhodopsin.

Acknowledgment. We thank Michael Gelb, Daniel Harries, Thomas Huber, and Jonathan N. Sachs for discussions and critical reading of the manuscript. H.I.P. gratefully acknowledges V. Adrian Parsegian for support and stimulating discussions. This research was supported by grants from the U. S. National Institutes of Health (IRTA Fellowship to H.I.P., GM27278 to T.J.M., and EY12049 to M.F.B.).

JA046453B

(71) Helfrich, W.; Servuss, R. *Nuovo Cimento D* **1984**, *3*, 137−151.